Available online at www.sciencedirect.com
SCIENCE DIRECT®
Acta Materialia 52 (2004) 1201–1209
Acta MATERIALIA
www.actamat-journals.com

Triple junction nanocracks in deformed nanocrystalline materials

I.A. Ovid'ko *, A.G. Sheinerman

Laboratory for Theory of Defects in Solids, Institute for Problems of Mechanical Engineering, Russian Academy of Sciences, Bolshoj 61, Vasil. Ostrov, St. Petersburg 199178, Russia

Received 22 September 2003; received in revised form 5 November 2003; accepted 5 November 2003

Abstract

A theoretical model is suggested which describes the generation and evolution of nanoscale cracks (nanocracks) at triple junctions of grain boundaries in deformed nanocrystalline materials. In the framework of the model, nanocracks in nanocrystalline materials are nucleated at triple junctions due to accumulation of the dislocation charge, that accompanies grain boundary sliding through triple junctions. The model accounts for experimental observation [Acta Mater. 51 (2003) 387] of triple junction nanocracks in deformed nanocrystalline Ni. With results of the model, the effects of grain boundary diffusion on suppression of nanocrack generation in nanocrystalline materials exhibiting enhanced ductility and superplasticity are discussed.

Keywords: Nanocrystalline materials; Grain boundaries; Mechanical properties; Superplasticity; Fracture

1. Introduction

The unique mechanical properties of nanocrystalline materials represent the subject of intensively growing fundamental and applied research; see, e.g., reviews [1–4]. Of special interest for a range of applications is the extremely high strength of nanocrystalline materials which are essentially stronger than their conventional coarse-grained counterparts [1–4]. However, in most cases, superstrong nanocrystalline materials exhibit low ductility, which limits their utility in many applications. At the same time, several examples of substantial tensile ductility and superplasticity in nanocrystalline materials have been reported recently [4–19]. With the experimental data discussed, it is very important to understand the fundamentals of failure processes responsible for brittle behavior of most nanocrystalline materials and analyse (super)plastic deformation mechanisms capable of effectively competing with these processes. In general, together with the conventional lattice dislocation slip, the plastic deformation mechanisms – grain boundary (GB) sliding [20–25], GB diffusional creep [26–29], triple junction diffusional creep [30], rotational deformation mode [24,31–33] – conducted by GB defects are treated to cause plastic flow in nanocrystalline materials. Also, following experimental data [5], nanovoids and nanocracks in ductile nanocrystalline Ni commonly nucleate and grow at GBs and their triple junctions during plastic deformation. In this context, with a very high volume fraction of triple junctions of GBs in nanocrystalline materials, of special interest are the mechanisms for nanocrack generation at triple junctions and their correlation with plastic deformation processes conducted by GB defects. The main aim of this paper is to suggest a theoretical model that describes nucleation and growth of nanocracks at triple junctions, induced by GB sliding through these junctions in deformed nanocrystalline materials. Also, we will discuss suppression of nanocrack generation at triple junctions due to the effects of diffusion processes.

2. Grain boundary sliding and generation of nanocracks at triple junctions of grain boundaries. Model

High-strain-rate superplastic deformation in nanocrystalline materials is characterized by strengthening at

* Corresponding author. Tel.: +7-812-321-4764; fax: +7-812-321-4771.
E-mail addresses: ovidko@def.ipme.ru (I.A. Ovid'ko), shein@def.ipme.ru (A.G. Sheinerman).

1359-6454/$30.00 © 2003 Acta Materialia Inc. Published by Elsevier Ltd. All rights reserved.
doi:10.1016/j.actamat.2003.11.004

first extended stage of deformation up to plastic strain degree ≈1–3 (100–300%) [13–19]. Also, the strengthening is often inherent to plastic deformation of nanocrystalline materials exhibiting a good ductility with plastic strain to failure $\varepsilon_f \approx 0.2$–$0.4$ [5]. The conventional lattice dislocation storage (causing strengthening in coarse-grained polycrystals) and deformationinduced grain growth are hardly responsible for the strengthening effect in nanocrystalline materials; see the discussion in [17,19]. In these circumstances, following model [25], the strengthening effect occurs owing to GB sliding in nanocrystalline materials, which leads to accumulation of sessile GB dislocations at triple junctions and the corresponding hampering of movement of mobile GB dislocations through dislocated triple junctions. We think that the sessile dislocations at triple junctions, that give rise to the experimentally observed [13–19] strengthening, are also responsible for the generation of triple junction nanocracks experimentally observed [5] in ductile nanocrystalline metals.

Let us discuss the scenario of the evolution of the defect structure, resulting in the generation of a triple junction nanocrack in mechanically loaded nanocrystalline materials. In doing so, with experimental observation [5] of lattice dislocations in ductile nanocrystalline Ni and experimental data [16,17] indicating on GB sliding and the existence of lattice dislocations in nanocrystalline materials under high-strain-rate superplastic deformation, we assume that both the GB sliding and conventional lattice dislocation slip cause plastic flow of a ductile nanocrystalline specimen. Following theoretical representations [23,25], GB dislocations – carriers of GB sliding – undergo transformations at triple junctions. Actually, when a mechanical load is applied to the specimen, mobile GB dislocations (with the Burgers vector being parallel to GB planes) move causing GB sliding (Fig. 1(a)). They are stopped at triple junctions of GBs, where GB planes are curved and thereby dislocation movement is hampered (Fig. 1(a)). At some critical shear stress, GB dislocations overcome triple junctions, in which case a sessile GB dislocation is formed at the triple junction (Fig. 1(b)) [25]. This process is an elementary act of (super)plastic deformation involving GB sliding in nanocrystalline materials characterized by a very high volume fraction of triple junctions. The process under consideration repeatedly occurs in a deformed nanocrystalline solid and is accompanied by an increase of the Burgers vector of the sessile dislocation at each step (Fig. 1(c) and (d)). We think that a nanocrack at the triple junction is generated to release the strain energy of the sessile GB dislocation resulted from numerous acts of GB sliding at the triple junction (Fig. 2). In doing so, mobile GB dislocations that carry GB sliding also influence the nanocrack generation (Fig. 2).

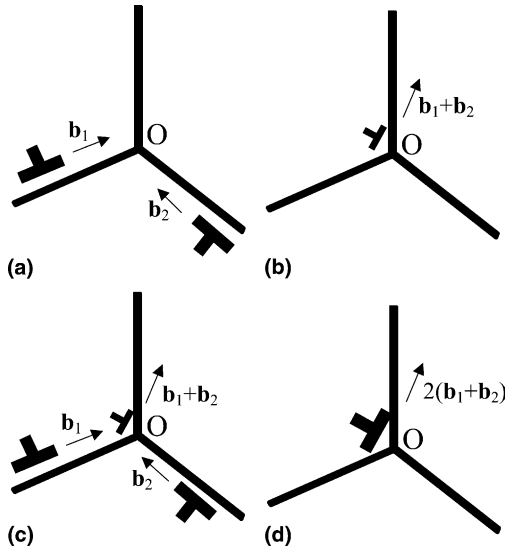

Fig. 1. Transformations of grain boundary dislocations – carriers of grain boundary sliding – at a triple junction. (a) Two gliding grain boundary dislocations with Burgers vectors $\boldsymbol{b}_1$ and $\boldsymbol{b}_2$ move towards the triple junction O. (b) Sessile dislocation with Burgers vector $\boldsymbol{b}_1 + \boldsymbol{b}_2$ is formed at triple junction. (c) Generation of two new gliding grain boundary dislocations that move towards the triple junction. (d) New sessile dislocation is formed which immediately converges with the first (see (b)) sessile dislocation at the triple junction.

Let us examine the energy characteristics of the generation of a triple junction nanocrack, which nucleates in the stress fields of the three GB dislocations with the Burgers vectors $\boldsymbol{b}_1$, $\boldsymbol{b}_2$ and $\boldsymbol{b}_3$ and the external stress σ^e_{ij} (Fig. 2). In the framework of our model, the nanocrack is assumed to be flat, and orientation of the nanocrack plane is arbitrary. That is, the nanocrack may nucleate either in grain interior (Fig. 2(a)) or along a GB adjacent to the triple junction (Fig. 2(b)).

For our analysis, we introduce the three rectangular coordinate systems (x, y), (x_1, y_1) and (x', y') as shown in Fig. 2. In doing so, the x-axis coincides with the direction of nanocrack plane growth (nucleation), and the x_1-axis coincides with the direction of the Burgers vector $\boldsymbol{b}_1$. In the chosen coordinate system (x', y'), the external stress tensor σ^e_{ij} has the only one non-zero component: $\sigma^e_{x'y'} = \tau$.

In the framework of our model, the geometric parameters of the defect configuration (Fig. 2) in question are as follows. The mobile GB dislocations with Burgers vectors $\boldsymbol{b}_1$ and $\boldsymbol{b}_2$ are distant by respectively l_1 and l_2 from the triple junction. The angle between GB planes containing these dislocations is β. Burgers vectors $\boldsymbol{b}_1$, $\boldsymbol{b}_2$ and $\boldsymbol{b}_3$ make angles α_1, α_2 and α_3, respectively, with the x-axis. The angle between the axes x' and x is γ (Fig. 2). The angles α_1, α_2, β and γ are in the following relationships: $\alpha_2 = \alpha_1 + \beta$, $\gamma = \alpha_1 + \beta/2 - \pi/2$. For simplicity, we also assume: $b_1 = b_2 = b$. In these circumstances, the

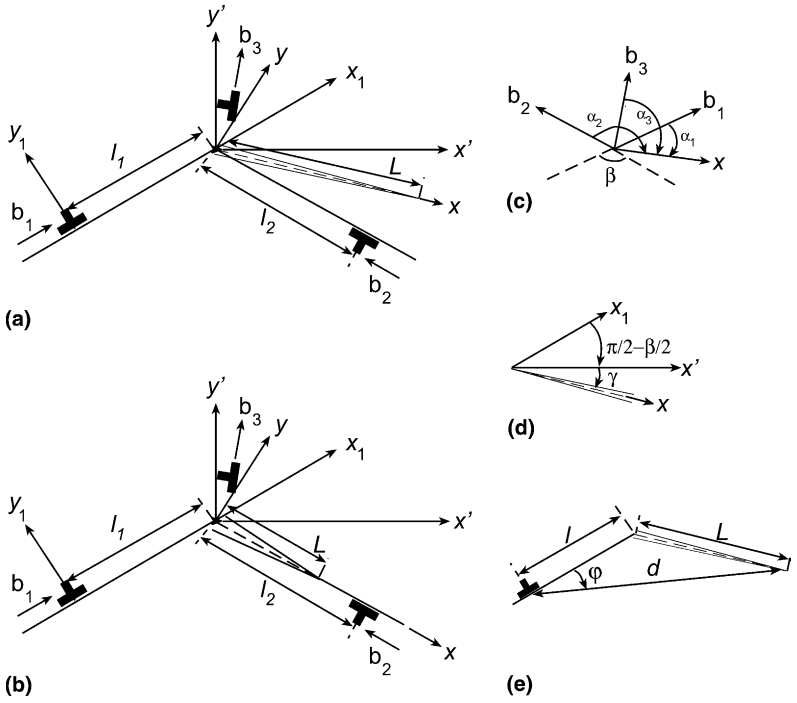

Fig. 2. Generation of flat nanocrack at a triple junction (a) in nanograin interior or (b) along a grain boundary plane. (c)–(e) Geometrical relationships between the parameters of the system.

following relationships are valid: $b_3 = 2nb\cos(\beta/2)$, and $\alpha_3 = \arccos(\frac{\cos\alpha_1+\cos\alpha_2}{2\cos(\beta/2)})$.

3. Equilibrium length of triple junction nanocrack

In order to quantitatively characterize the nanocrack generation, we will calculate in the first approximation the equilibrium length L_e of a nanocrack. In the situation discussed (Fig. 2), the equilibrium length of the nanocrack is defined as that corresponding to the minimum energy of the system (for details, see below). In calculation of L_e, we will use the configurational force method [34] effectively exploited in analysis of the generation of plane microcracks in the stress fields of superdislocations [34], dislocation pile-ups [34], disclination loops [35], lamellar terminations in eutectics [36] and wedge line disclinations [37]. Following [34], the configurational force F is defined as the elastic energy released when the crack moves over a unit distance. In the situation with the plane strain state of an elastically isotropic solid, examined in this paper, F can be written in its general form as follows [34]:

$$F = \frac{\pi(1-\nu)L}{4G}\left(\bar{\sigma}_{yy}^2 + \bar{\sigma}_{xy}^2\right), \tag{1}$$

where G is the shear modulus, ν is the Poisson ratio, and $\bar{\sigma}_{yy}$ and $\bar{\sigma}_{xy}$ are the mean weighted values of the stress tensor components σ_{yy} and σ_{xy}, respectively. These mean weighted stress tensor components are calculated using the following formula [34]:

$$\bar{\sigma}_{iy} = \frac{2}{\pi L}\int_0^L \sigma_{iy}(x, y=0)\sqrt{\frac{x}{L-x}}\,\mathrm{d}x, \quad i = x, y. \tag{2}$$

The equilibrium length L_e of the nanocrack is derived from the balance $F = 2\gamma_e$ between the release F of the elastic energy and the formation of two new nanocrack surfaces characterized by the surface energy density γ_e per unit area. Here $\gamma_e = \gamma$, the surface energy density per unit area of the free surface, when the nanocrack nucleates in the grain interior (Fig. 2(a)), and $\gamma_e = \gamma - \gamma_s/2$, when the nanocrack nucleates along a GB (Fig. 2(b)) characterized by the energy density γ_s per unit area of GB plane. The nucleation of the triple junction nanocrack (Fig. 2) is energetically favorable, if $F > 2\gamma_e$, and unfavorable, if $F < 2\gamma_e$.

Let us calculate the stress tensor components σ_{xy} and σ_{yy} figuring in formula (2). Each component contains the four constituent terms:

$$\sigma_{iy} = \sigma_{iy}^{b_1} + \sigma_{iy}^{b_2} + \sigma_{iy}^{b_3} + \sigma_{iy}^{e}, \tag{3}$$

where $i = x, y$, σ_{iy}^{e} is the external stress, and $\sigma_{iy}^{b_1}$, $\sigma_{iy}^{b_2}$ and $\sigma_{iy}^{b_3}$ are the stress fields created by GB dislocations with Burgers vectors $\boldsymbol{b}_1$, $\boldsymbol{b}_2$ and $\boldsymbol{b}_3$, respectively. With (3) substituted to formula (2), we have:

$$\bar{\sigma}_{iy} = \bar{\sigma}_{iy}^{b_1} + \bar{\sigma}_{iy}^{b_2} + \bar{\sigma}_{iy}^{b_3} + \bar{\sigma}_{iy}^{e}, \tag{4}$$

where $\bar{\sigma}_{iy}^{b_k}$ $(k=1,2,3)$ and $\bar{\sigma}_{iy}^{e}$ are the mean weighted values of the stress field components $\sigma_{iy}^{b_k}$ and σ_{iy}^{e}, respectively.

In order to calculate the stresses $\sigma_{iy}^{b_1}$, we write the expressions [38] for the stress field components $\sigma_{ij}^{b_1}$ created by the dislocation the with Burgers vector $\boldsymbol{b}_1$ in the coordinate system (x_1, y_1). In doing so, we have:

$$\sigma_{x_1x_1}^{b_1} = -Db_1 \frac{y_1(3x_1^2+y_1^2)}{r_1^4}, \tag{5}$$

$$\sigma_{y_1y_1}^{b_1} = Db_1 \frac{y_1(x_1^2-y_1^2)}{r_1^4}, \tag{6}$$

$$\sigma_{x_1y_1}^{b_1} = Db_1 \frac{x_1(x_1^2-y_1^2)}{r_1^4}, \tag{7}$$

where $D = G/[2\pi(1-\nu)]$, and $r_1^2 = x_1^2+y_1^2 = x^2 + 2l_1x\cos\alpha_1 + l_1^2$. The stress field components $\sigma_{yy}^{b_1}$ and $\sigma_{xy}^{b_1}$ of the dislocation under consideration are expressed through the stresses $\sigma_{x_1x_1}^{b_1}$, $\sigma_{y_1y_1}^{b_1}$ and $\sigma_{x_1y_1}^{b_1}$ as follows:

$$\sigma_{yy}^{b_1} = \sigma_{x_1x_1}^{b_1}\sin^2\alpha_1 + \sigma_{y_1y_1}^{b_1}\cos^2\alpha_1 + \sigma_{x_1y_1}^{b_1}\sin 2\alpha_1, \tag{8}$$

$$\sigma_{xy}^{b_1} = \tfrac{1}{2}\left(\sigma_{x_1x_1}^{b_1} - \sigma_{y_1y_1}^{b_1}\right)\sin 2\alpha_1 + \sigma_{x_1y_1}^{b_1}\cos 2\alpha_1. \tag{9}$$

In their turn, the coordinates x_1 and y_1 are in the following relationships with x and y:

$$\begin{aligned} x_1 &= l_1 + x\cos\alpha_1 + y\sin\alpha_1, \\ y_1 &= -x\sin\alpha_1 + y\cos\alpha_1. \end{aligned} \tag{10}$$

With (5)–(7) and (10) substituted to formulas (8) and (9), we find:

$$\begin{aligned} &\sigma_{yy}^{b_1}(x, y=0) \\ &\quad = Db_1\sin\alpha_1\left\{\frac{2l_1\cos\alpha_1}{r_1^2} + (2-\cos 2\alpha_1)\frac{x}{r_1^2}\right. \\ &\qquad \left. - 2l_1\sin 2\alpha_1\sin\alpha_1\frac{x^2}{r_1^4} - 2\sin^2\alpha_1\frac{x^3}{r_1^4}\right\}, \end{aligned} \tag{11}$$

$$\begin{aligned} &\sigma_{xy}^{b_1}(x, y=0) \\ &\quad = Db_1\left\{\frac{l_1\cos 2\alpha_1}{r_1^2} + (2-\cos 2\alpha_1)\cos\alpha_1\frac{x}{r_1^2}\right. \\ &\qquad \left. - 2l_1\sin^2\alpha_1\cos 2\alpha_1\frac{x^2}{r_1^4} - 2\sin^2\alpha_1\cos\alpha_1\frac{x^3}{r_1^4}\right\}. \end{aligned} \tag{12}$$

The mean weighted values $\bar{\sigma}_{iy}^{b_1} = \frac{2}{\pi L}\int_0^L \sigma_{iy}^{b_1}(x, y=0)\sqrt{\frac{x}{L-x}}\mathrm{d}x$ of the stresses $\sigma_{iy}^{b_1}$ are obtained by integration of expressions (11) and (12). They read: $\bar{\sigma}_{iy}^{b_1} = (Db_1/L)g_{iy}(l_1, \alpha_1)$, where

$$\begin{aligned} &g_{yy}(l,\alpha) \\ &\quad = \sin\alpha\left\{2 + \sqrt{\frac{l}{d}}\left[\frac{\tilde{l}\cos(\alpha-\varphi/2)+\cos(\varphi/2)}{\tilde{d}^2} - 2\cos\frac{\varphi}{2}\right]\right\}, \end{aligned} \tag{13}$$

$$\begin{aligned} g_{xy}(l,\alpha) &= 2\cos\alpha\left(1 - \sqrt{\frac{l}{d}}\cos\frac{\varphi}{2}\right) \\ &\quad + \sqrt{\frac{l}{d}}\frac{\sin(\varphi/2) - \tilde{l}\sin(\alpha-\varphi/2)}{\tilde{d}^2}\sin\alpha, \\ &\quad -\pi < \alpha \leqslant \pi. \end{aligned} \tag{14}$$

In formulas (13) and (14), we have used the following designations: $d = (l^2 + 2lL\cos\alpha + L^2)^{1/2}$, $\varphi = \arctan\frac{\sin\alpha}{l+\cos\alpha} + \pi\Theta(-\tilde{l}-\cos\alpha)\operatorname{sign}\alpha$, $\tilde{l} = l/L$, and $\tilde{d} = d/L$. $\Theta(x)$ is the Heaviside function ($\Theta(x) = 1$, if $x > 0$, and $= 0$, if $x < 0$). The geometric interpretation of the parameters d and φ is evident from Fig. 2(e).

The mean weighted values $\bar{\sigma}_{iy}^{b_2}$ and $\bar{\sigma}_{iy}^{b_3}$ of the stress field components $\sigma_{iy}^{b_2}$ and $\sigma_{iy}^{b_3}$, respectively, are calculated in the same way as $\bar{\sigma}_{iy}^{b_1}$. In doing so, we find: $\bar{\sigma}_{iy}^{b_2} = (Db_2/L)g_{iy}(l_2, \alpha_2)$, and $\bar{\sigma}_{iy}^{b_3} = (Db_3/L)g_{iy}(0, \alpha_3)$. In order to calculate $\bar{\sigma}_{iy}^{e}$, we will write the components σ_{yy}^{e} and σ_{xy}^{e} in the coordinate system (x, y) as follows: $\sigma_{yy}^{e} = \tau\sin 2\gamma$, and $\sigma_{xy}^{e} = \tau\cos 2\gamma$. Since the stresses σ_{iy}^{e} are constant, we have: $\bar{\sigma}_{iy}^{e} = \frac{2}{\pi L}\int_0^L \sigma_{iy}^{e}\sqrt{\frac{x}{L-x}}\mathrm{d}x = \sigma_{iy}^{e}$. As a corollary, one finds $\bar{\sigma}_{yy}^{e} = \tau\sin 2\gamma$, and $\bar{\sigma}_{xy}^{e} = \tau\cos 2\gamma$.

With the above formulas for $\bar{\sigma}_{iy}^{b_1}$, $\bar{\sigma}_{iy}^{b_2}$, $\bar{\sigma}_{iy}^{b_3}$ and $\bar{\sigma}_{iy}^{e}$ and formula (4) substituted to formula (1), and conditions $b_1 = b_2 = b$ and $b_3 = 2nb\cos(\beta/2)$ taken into account, we get the following expression for the configurational force F:

$$\begin{aligned} F &= \frac{Gb^2}{16\pi(1-\nu)L} \\ &\quad \times \left\{\left(g_{yy}(l_1,\alpha_1) + g_{yy}(l_2,\alpha_2) + g_{yy}(0,\alpha_3)\right.\right. \\ &\qquad \left. + \frac{\tau L}{2\pi(1-\nu)Gb}\sin 2\gamma\right)^2 + \left(g_{xy}(l_1,\alpha_1) + g_{xy}(l_2,\alpha_2)\right. \\ &\qquad \left.\left. + g_{xy}(0,\alpha_3) + \frac{\tau L}{2\pi(1-\nu)Gb}\cos 2\gamma\right)^2\right\}. \end{aligned} \tag{15}$$

4. Results of model

The dependences of F (in units of $Gb/[16\pi(1-\nu)]$) on non-dimensional length L/b of the nanocrack, given by formula (15), are shown in Fig. 3, for $\beta = 2\pi/3$, $\tau/G = 0.01$, $l_1 = l_2 = 100b$, $\nu = 0.3$ and different values of n and α_1. The horizontal lines show values of the effective surface energy density $2\gamma_e$ (in units of $Gb/[16\pi(1-\nu)]$) in the cases of the nanocrack nucleat-

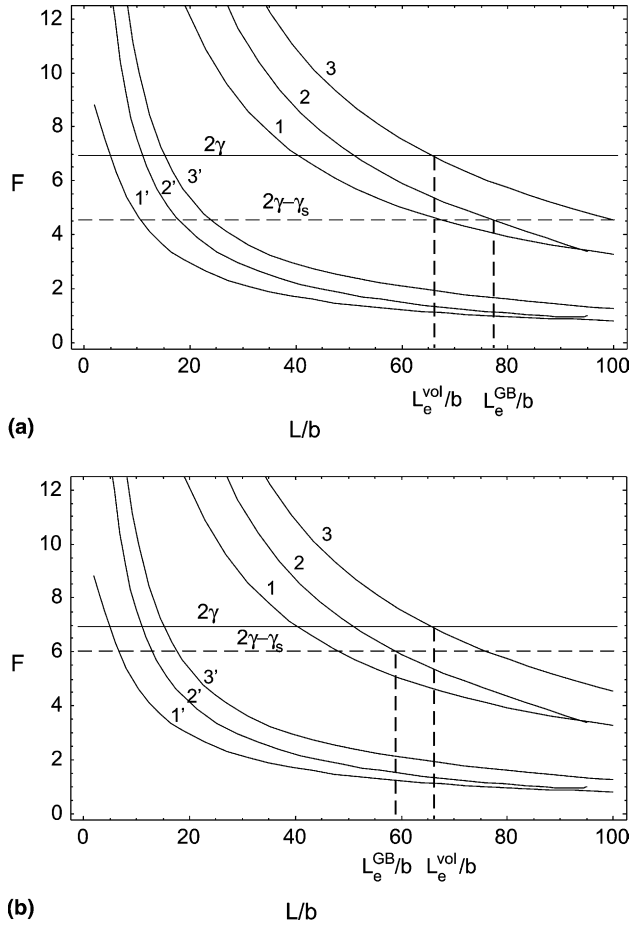

Fig. 3. Dependence of the configurational force F (in units of $Gb/[16\pi(1-\nu)]$) on non-dimensional length L/b of the nanocrack, for $\beta = 2\pi/3$, $\tau/G = 0.01$, $l_1 = l_2 = 100b$, $\nu = 0.3$; $n = 10$ and $\alpha_1 = -\pi/3$, $\pi/3$ and $2\pi/3$ (see curves 1, 2 and 3, respectively) as well as $n = 5$ and $\alpha_1 = -\pi/3$, $\pi/3$ and $2\pi/3$ (see curves $1'$, $2'$ and $3'$, respectively). Horizontal lines show values of the effective surface energy density $2\gamma_e$ (in units of $Gb/[16\pi(1-\nu)]$) in the cases of the nanocrack nucleating in the grain interior (solid line) and along GB plane (dashed line), for $\gamma/(Gb) = 0.1$ and (a) $\gamma_s/(Gb) = 0.07$ and (b) $\gamma_s/(Gb) = 0.03$.

ing in the grain interior (solid line) and along a GB plane (dashed line), shown in Fig. 2(a) and (b), respectively. The generation of the nanocrack in the grain interior is energetically favorable in the range of parameters where the curve $F(L/b)$ lies above the solid line in Fig. 3. The generation of the nanocrack along a GB plane is energetically favorable in the range of parameters where the curve $F(L/b)$ lies above the dashed line in Fig. 3. The equilibrium length of the nanocrack corresponds to the point where the curve $F(L/b)$ and the horizontal line (solid line in the case of the nanocrack in the grain interior, and dashed line in the case of the nanocrack nucleating along a GB plane) intersect. In Fig. 3, the equilibrium length of the nanocrack in grain interior and along a GB is denoted as L_e^{vol} and L_e^{GB}, respectively. For $L < L_e$, the nanocrack growth is energetically favorable until its length L reaches L_e.

Notice that the growth of a triple junction nanocrack (Fig. 2) is energetically favorable in the only case where its length is lower than its equilibrium value. It is contrasted to the situation with microcracks generated in either the external constant stress field or the stress fields of disclinations [37] (rotational defects which are typical structural elements of non-equilibrium GBs [39–42] and carriers of rotational deformation in poly- and nanocrystalline materials [24,31–33,40]). Such a microcrack starts to rapidly grow, if its length is larger than some critical value. In contrast, the formation of a triple junction nanocrack (Fig. 2) with the length $L > L_e$ is energetically unfavorable. The stable state of the nanocrack is characterized by $L = L_e$ that corresponds to the minimum energy of the system. This feature of triple junction nanocracks generated in the stress field of a sessile GB (super)dislocation is related to the fact that the dislocation stress field rapidly falls with increasing distance from the dislocation line, while the external stress τ weakly influences the nanocrack generation. (Analysis shows that the external stress τ is low compared to the dislocation stress field at distances $\leqslant d$ (with d being the grain size) from the dislocated triple junction.)

The notion of a nanocrack (or, more generally, crack) has its sense when the nanocrack length is larger than some critical minimum length $L_c \approx 5a \approx 15b$ (with a being the crystal lattice parameter) at which the binding between the atoms of the opposite surfaces of the nanocrack is completely broken. In this context, we treat the generation of a nanocrack to occur, if its equilibrium length $L_e \geqslant L_c$. In the opposite case ($L_e < L_c$), the binding between the atoms of the opposite surfaces of the nanocrack causes it to shrink and disappear.

The dependences of the equilibrium length L_e of a triple junction nanocrack on the parameter n (characterizing the Burgers vector of the sessile GB (super)dislocation and plastic strain degree) are shown in Fig. 4

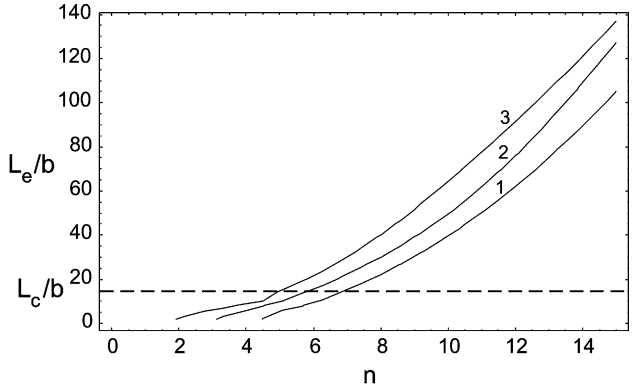

Fig. 4. Dependencies of non-dimensional equilibrium nanocrack length L_e/b on parameter n, for $\beta = 2\pi/3$, $\tau/G = 0.01$, $l_1 = l_2 = 100b$, $\nu = 0.3$; $\alpha_1 = -\pi/3$, 0 and $2\pi/3$ (see curves 1, 2 and 3, respectively). The dashed horizontal line corresponds to the minimum critical length $L_c = 15b$ at which the nanocrack is generated.

for different values of the angle α_1. As follows from Figs. 3 and 4, the equilibrium length L_e rapidly increases with rising parameter n in both the cases of the nanocrack growing in the grain interior and along a GB. The dashed horizontal line in Fig. 4 corresponds to the critical minimum length $L_e = 15b$ of a nanocrack. The points where this horizontal line intersects the curves $L_e(n)$ correspond to the values of n at which the nanocracks are generated. These values are close to 5, indicating that a stable nanocrack is nucleated at a triple junction after just several (about 5) acts of the GB dislocation transformation (Fig. 2) have occurred at the triple junction. Also, as follows from Fig. 3, L_e grows when the angle β between GB planes decreases, because b_3 grows with decreasing β as well. At the same time, the equilibrium length L_e rapidly falls with rising the surface energy density γ_e.

In Fig. 5, the equilibrium lengths L_e^{vol} of nanocracks are plotted as functions of the angle α_1 for $n = 5$ (curve 1) and $n = 10$ (curve 2). As follows from Figs. 3 and 5, the equilibrium length L_e of the nanocrack (growing either in a grain interior or along a GB) is highly sensitive to the angle α_1 that characterizes orientation of the nanocrack plane. For the triple junction nanocrack growing along a GB plane, the angle α_1 is determined by geometry of the triple junction and its adjacent GBs. (Curves 2 and 2′ in Fig. 3 show dependences $F(L/b)$, for such a nanocrack with $\alpha_1 = \pi/3$). In these circumstances, the equilibrium length L_e^{GB} of a nanocrack nucleating along a GB plane can be either larger or lower than the equilibrium length of a nanocrack nucleating in grain interior. The former case ($L_e^{GB} > L_e^{vol}$) illustrated in Fig. 3(a) is realized at large values of the GB energy density γ_s. In doing so, the nucleation of the triple junction nanocrack growing along a GB is energetically preferred compared to the nanocrack growing in grain interior. The second case ($L_e^{GB} < L_e^{vol}$) illustrated in Fig. 3(b) is realized at low values of γ_s. In this case, the nucleation of the triple junction nanocrack growing in grain interior is preferred.

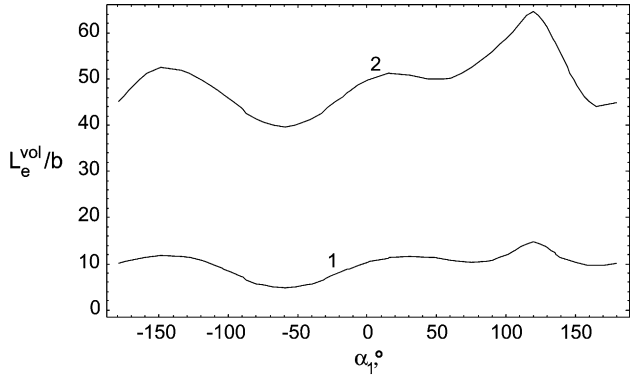

Fig. 5. Dependencies of non-dimensional equilibrium nanocrack length L_e^{vol}/b on angle α_1, for $\beta = 2\pi/3$, $\tau/G = 0.01$, $l_1 = l_2 = 100b$, $\nu = 0.3$; $n = 5$ and 10 (see curves 1 and 2, respectively).

5. Effects of diffusion on nanocrack generation

In a nanocrystalline material characterized by a distribution in grain size, different deformation mechanisms operate which are the conventional lattice dislocation slip, the GB sliding, Coble creep, triple junction diffusional creep and rotational deformation [20–33]. These mechanisms compete with each other and nanocrack generation in releasing the internal stresses and thus cause the deformation behavior of the material. In doing so, diffusion processes in nanocrystalline materials are capable of strongly affecting the competition between different deformation and failure mechanisms. At the same time, diffusion is crucially influenced by action of these mechanisms. A detailed analysis of the very complicated relationships between deformation, failure and diffusion processes is beyond the scope of this paper focused on nucleation and evolution of triple junction nanocracks. Here, with results of our theoretical model, we will briefly discuss only the effects of diffusion on suppression of the nucleation of triple junction nanocracks in deformed nanocrystalline materials.

GB diffusion can be highly enhanced in nanocrystalline materials due to the action of lattice dislocation slip which "supplies" dislocations to GBs where these trapped dislocations climb, split into GB dislocations and annihilate causing the intensive generation of excess GB point defects that carry GB diffusion [43–45] (Fig. 6). The enhanced GB diffusion gives rise to the three following effects responsible for suppression of nucleation of triple junction nanocracks: (i) Sessile dislocations formed at triple junctions due to GB sliding intensively climb towards each other and annihilate (Fig. 7), in which case they stop to be the stress sources initiating the nucleation of nanocracks. (The rate of the dislocation climb is controlled by diffusion and thereby highly enhanced in nanocrystalline materials with high diffusion coefficients.) (ii) The enhanced diffusion provides intensive movement of interstitial atoms to the local regions where high tensile stresses of the sessile triple junction dislocations exist (Fig. 8). In these circumstances, the tensile stresses, in part, are relaxed, and the nucleation of nanocracks is hampered. (iii) The enhanced GB diffusion provides the effective action of Coble creep [26–29] and triple junction diffusional creep [30] which thereby effectively compete with GB sliding. As a corollary, the contribution of GB sliding to plastic flow decreases, in which case growth of Burgers vectors of the sessile dislocations – nuclei of triple junction nanocracks (Fig. 2) – slows down or stops.

We think that these three effects of GB diffusion (enhanced owing to the action of conventional lattice dislocation slip) give rise to enhanced ductility exhibited by nanocrystalline Ni [5] and materials with bimodal (nano-plus micro-grained) structures [46], as well as to

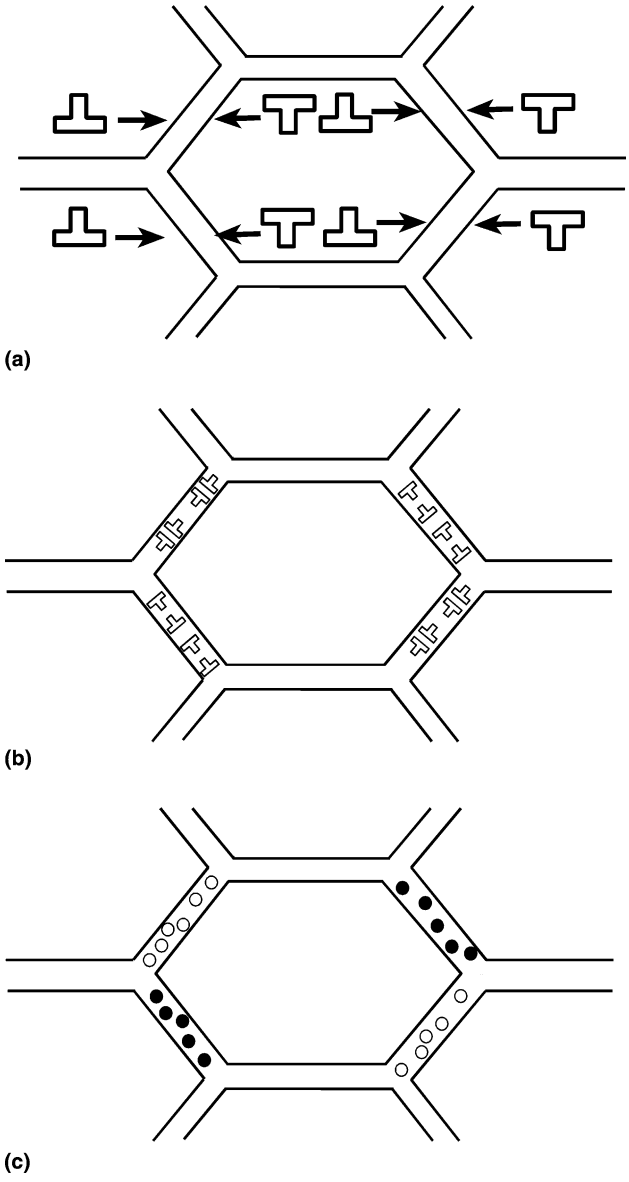

Fig. 6. Enhancement of grain boundary diffusion due to absorption of lattice dislocations by grain boundaries (schematically). (a) Lattice dislocations (large open dislocation signs) move under the shear stress action. (b) Climbing dislocations (small open dislocation signs) resulted from splitting of absorbed lattice dislocations form dipole configurations at grain boundaries. (c) Annihilation of climbing dislocations forming dipole configurations results in the formation of high-density ensembles of non-equilibrium point defects – vacancies (open circles) and interstitials (full circles) – that carry enhanced grain boundary diffusion.

high-strain-rate superplasticity exhibited by nanocrystalline materials [11–19]. In doing so, the combined action of lattice dislocation slip and GB sliding as dominant deformation modes is crucial. These deformation modes cause mutually consistent plastic flow of both grain interiors and GBs. In addition, the lattice dislocation slip provides "bombardment" of GBs by lattice dislocations which lead to enhancement of GB diffusion (Fig. 6). The enhanced diffusion suppresses

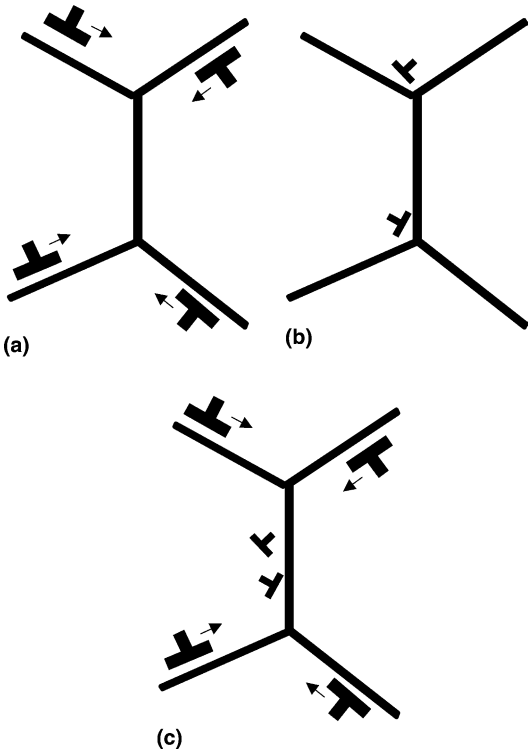

Fig. 7. Sessile dislocations generated (due to grain boundary sliding) at neighbouring triple junctions climb towards each other.

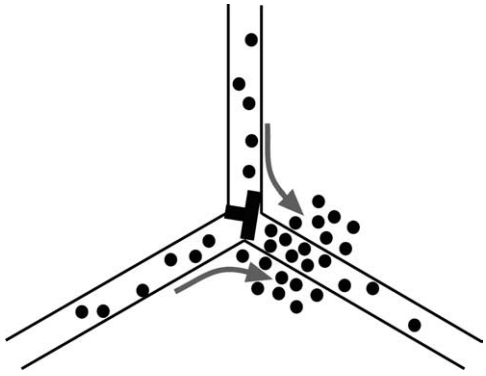

Fig. 8. Diffusional flow of interstitial atoms causes a partial relaxation of tensile stresses created by triple junction dislocation.

nucleation of GB-sliding-induced nanocracks in nanocrystalline materials which threreby exhibit a good ductility or even superplasticity.

6. Concluding remarks

In this paper, it has been theoretically revealed that the nucleation of nanocracks in deformed nanocrystalline materials can effectively occur at triple junctions (Fig. 2) due to GB sliding. The driving force of the nucleation of triple junction nanocracks is the release of the elastic energy associated with the GB-sliding-induced

storage of GB dislocations at triple junctions. A triple junction nanocrack (Fig. 2) is characterized by the equilibrium length L_e that corresponds to the stable, low-energy state of the nanocrack. The equilibrium length L_e is highly sensitive to the parameters characterizing the triple junction geometry, the specific energy of the nanocrack surface, and GB dislocation storage at the triple junction. In particular, triple junction nanocracks nucleate and rapidly grow with rising the Burgers vectors of GB dislocations generated and accumulated at triple junctions due to GB sliding. More precisely, a stable nanocrack is nucleated at a triple junction after just several (about 5) acts of the GB dislocation transformation (Fig. 2) have occurred at the triple junction. In contrast, enhanced diffusion processes are capable of suppressing the nanocrack generation at triple junctions in mechanically loaded nanocrystalline materials in which the lattice dislocation slip (causing increase of GB diffusion coefficient) and GB sliding act as dominant deformation mechanisms.

The theoretical model suggested in this paper accounts for experimental observation [5] of nanocracks nucleated at triple junctions in deformed nanocrystalline Ni samples exhibiting a substantial ductility. These samples were fabricated by electrodeposition methods, taking care about absence of nanocracks and nanopores in as-prepared state. Therefore, triple junction nanocracks observed by Kumar et al. [5] in "in-situ" experiments during plastic deformation in nanocrystalline Ni are definitely induced by deformation processes. Notice that our model predicts a certain stability of triple junction nanocracks. This prediction is in agreement with experiments [5] in which a good ductility of deformed nanocrystalline materials and a non-catastrophic character of failure processes have been detected. Also, lattice dislocation slip and GB sliding have been identified as dominant deformation modes in nanocrystalline materials exhibiting a substantial ductility [5] and superplasticity [17,19]. This corresponds to basic statements of our model, because the lattice dislocation slip supplies lattice dislocations to GBs where they split into sessile and mobile GB dislocations. These mobile GB dislocations move through triple junctions and cause the dislocation charge storage (Fig. 1) followed by nanocrack nucleation (Fig. 2) at these junctions. In this context, however, it should be noted that the suggested mechanism for nucleation of triple junction nanocracks may be not effective in nanocrystalline materials with the very fine grain sizes $d < 30$ nm. Actually, lattice dislocation slip is suppressed in very small nanograins [47,48], in which case it can not support intense GB sliding. In addition, GB dislocation pile-ups can not be sustained in nanocrystalline materials with very fine grain sizes. As a corollary, movement of GB dislocations through triple junctions is hampered in such materials, compared to nanocrystalline materials with relatively large grains where the stress concentration at GB dislocation pile-up heads enhances movement of GB dislocations through triple junctions [23].

Finally, notice that the suggested model is effective in a description of failure processes in mesoscale ceramic crystals where lattice slip is suppressed but GB sliding is allowed (for details, see [49] and references therein). The cracks at triple junctions of grain boundaries in such mesoscale crystals are able to nucleate due to GB sliding in the same way as triple junction nanocracks in nanocrystalline materials (Fig. 2).

Acknowledgements

This work was supported, in part, by the Office of US Naval Research (Grant N00014-01-1-1020), "Integration" Program (grant B0026), the Russian Fund of Basic Research, Russian Academy of Sciences Program "Structural Mechanics of Materials and Constructions", and St. Petersburg Scientific Center. Many thanks are due to Dr. Mikhail Gutkin for helpful discussions.

References

[1] Koch CC, Morris DG, Lu K, Inoue A. MRS Bull 1999;24:54.
[2] Mohamed FA, Li Y. Mater Sci Eng A 2001;298:1.
[3] Padmanabhan KA. Mater Sci Eng A 2001;304–306:200.
[4] Zhan G-D, Kuntz JD, Wan J, Mukherjee AK. In: Berndt CC, Fischer T, Ovid'ko IA, Skandan G, Tsakalakos T, editors. Nanomaterials for structural applications. MRS Symp Proc vol 740. Warrendale: MRS, 2003. p. 41.
[5] Kumar KS, Suresh S, Chisholm MF, Horton JA, Wang P. Acta Mater 2003;51:387.
[6] Mayo MJ. Nanostruct Mater 1997;9:717.
[7] Champion Y, Lahglois C, Guerin-Mailly S, Langlois P, Bonnentien J-L, Hytch M. Science 2003;300:310.
[8] Wang Y, Chen M, Zhou F, Ma E. Nature 2002;419:912.
[9] He G, Eckert J, Loeser W, Schultz L. Nature Mater 2003;2:33.
[10] Ma E. Nature Mater 2003;2:7.
[11] Mishra RS, Valiev RZ, McFadden SX, Mukherjee AK. Mater Sci Eng A 1998;252:174.
[12] McFadden SX, Misra RS, Valiev RZ, Zhilyaev AP, Mukherjee AK. Nature 1999;398:684.
[13] Islamgaliev RK, Valiev RZ, Mishra RS, Mukherjee AK. Mater Sci Eng A 2001;304–306:206.
[14] Mishra RS, Valiev RZ, McFadden SX, Islamgaliev RK, Mukherjee AK. Philos Mag A 2001;81:37.
[15] Mishra RS, Stolyarov VV, Echer C, Valiev RZ, Mukherjee AK. Mater Sci Eng A 2001;298:44.
[16] Valiev RZ, Song C, McFadden SX, Mukherjee AK, Mishra RS. Philos Mag A 2001;81:25.
[17] Mukherjee AK. Mater Sci Eng A 2002;322:1.
[18] Valiev RZ, Alexandrov IV, Zhu YT, Lowe TC. J Mater Res 2002;17:5.
[19] Mukherjee AK. In: Mishra RS, Earthman JC, Raj SV, editors. Creep Deformation: Fundamentals and Applications. Warrendale: TMS; 2002. p. 3.
[20] Hahn H, Mondal P, Padmanabhan KA. Nanostruct Mater 1997;9:603.

[21] Hahn H, Padmanabhan KA. Phil Mag B 1997;76:559.
[22] Konstantinidis DA, Aifantis EC. Nanostruct Mater 1998;10:1111.
[23] Fedorov AA, Gutkin MYu, Ovid'ko IA. Acta Mater 2003;51:887.
[24] Gutkin MYu, Ovid'ko IA, Skiba NV. Acta Mater 2003;51:4059.
[25] Gutkin MYu, Ovid'ko IA, Skiba NV. J Phys D 2003;36:L47.
[26] Masumura RA, Hazzledine PM, Pande CS. Acta Mater 1998;46:4527.
[27] Kim HS, Estrin Y, Bush MB. Acta Mater 2000;48:493.
[28] Yamakov V, Wolf D, Phillpot SR, Gleiter H. Acta Mater 2002;50:61.
[29] Masumura RA, Pande CS. In: Berndt CC, Fischer T, Ovid'ko IA, Skandan G, Tsakalakos T, editors. Nanomaterials for structural applications, MRS Symp Proc. vol. 740. Warrendale: MRS, 2003. p. 3.
[30] Fedorov AA, Gutkin MYu, Ovid'ko IA. Scripta Mater 2002;47:51.
[31] Murayama M, Howe JM, Hidaka H, Takaki S. Science 2002;295:2433.
[32] Ovid'ko IA. Science 2002;295:2386.
[33] Gutkin MYu, Kolesnikova AL, Ovid'ko IA, Skiba NV. Philos Mag Lett 2002;81:651.
[34] Indenbom VI. Fiz Tverd Tela 1961;3:2071 (trans. in Sov Phys Solid State).
[35] Rybin VV, Zhukovskii IM. Phys Tverd Tela 1978;20:1829 (trans. in Sov Phys Solid State).
[36] Vladimirov VI, Gutkin MYu, Romanov AE. Mech Compos Mater 1987;23:313.
[37] Gutkin MYu, Ovid'ko IA. Philos Mag 1994;70:561.
[38] Hirth JP, Lothe J. Theory of dislocations. New York: John Wiley; 1982.
[39] Nazarov AA, Romanov AE, Valiev RZ. Acta Metall Mater 1993;41:1033.
[40] Klimanek P, Klemm V, Romanov AE, Seefeldt M. Adv Eng Mater 2001;3:877.
[41] Gutkin MYu, Ovid'ko IA. Phys Rev B 2001;63:064515.
[42] Bobylev SV, Ovid'ko IA, Sheinerman AG. Phys Rev B 2001;64:224507.
[43] Zelin MG, Mukherjee AK. Mater Sci Eng A 1996;208:210.
[44] Valiev RZ, Alexandrov IV. Nanostructured materials prepared by severe plastic deformation. Moscow: Logos; 2000 [in Russian].
[45] Ovid'ko IA, Sheinerman AG. Philos Mag 2003;83:1551.
[46] Wang Y, Chen M, Zhou F, Ma E. Nature 2002;419:912.
[47] Gryaznov VG, Polonsky IA, Romanov AE, Trusov LI. Phys Rev B 1991;44:42.
[48] Weertman JR, Sanders PG. Solid State Phenom 1994;35–36:249.
[49] Evans AG, Rice JR, Hirth JP. J Am Ceram Soc 1980;63:368.